ACS APPLIED NANO MATERIALS

www.acsanm.org Article

Cobalt-Doped Zinc Oxide Nanoparticle–MoS_2 Nanosheet Composites as Broad-Spectrum Bactericidal Agents

Junli Liu,* Wenxia Cheng, Yuhan Wang, Xiuyi Fan, Jiahao Shen, Hui Liu, Aiqin Wang, Aiping Hui, Forrest Nichols, and Shaowei Chen*

Cite This: *ACS Appl. Nano Mater.* 2021, 4, 4361–4370 Read Online

ACCESS | Metrics & More | Article Recommendations | Supporting Information

ABSTRACT: The design and engineering of high-performance antimicrobial agents is critical for combating antibiotic resistance. In the present study, a rapid and broad-spectrum bactericidal agent is developed based on nanocomposites consisting of cobalt-doped zinc oxide (CoZnO) nanoparticles and MoS_2 nanosheets. The CoZnO/MoS_2 nanocomposites are prepared by a facile chemical precipitation method at controlled CoZnO and MoS_2 feeds. Scanning and transmission electron microscopic measurements show that CoZnO nanoparticles (ca. 10 nm in diameter) are clustered on the MoS_2 nanosheet surface, which facilitates the charge separation of the photo-generated electron–hole pairs, leading to enhanced photodynamic antimicrobial activity. Antibacterial assays in the dark show that the CoZnO/MoS_2 nanocomposite prepared at 30 μg of MoS_2 feed (CoZnO/MoS_2-30) exhibits the best performance among a series of samples, with minimum inhibitory concentrations of 0.25, 0.8, and 1.8 mg mL^{-1} toward the Gram-negative bacterium *Escherichia coli*, Gram-positive bacterium *Staphylococcus aureus* and fungus *Aspergillus flavus*, respectively. The antibacterial performance is markedly enhanced under photoirradiation, where 94.0% inactivation of *E. coli* is achieved with 20 μg mL^{-1} CoZnO/MoS_2-30 nanocomposite under photoirradiation (15 W, 360 nm) for 5 min. The high antibacterial activity can be ascribed to peroxidase-like photocatalytic activity that is conducive to the generation of reactive oxygen species, as evidenced in transmission electron microscopy, electron spin resonance, and intracellular glutathione oxidation measurements. The results of the present study highlight the significance of CoZnO/MoS_2 nanocomposites as potent photodynamic antibacterial agents.

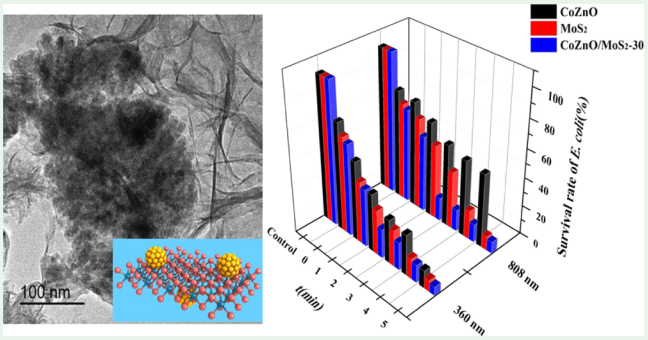

KEYWORDS: *CoZnO/MoS_2 nanocomposite, broad-spectrum bacteria inhibition, photocatalysis, peroxidase activity, photodynamics*

1. INTRODUCTION

Bacterial infections are increasingly recognized as a major threat to the well-being of humankind, and the indiscriminate use of antibiotics has contributed to the emergence of "superbugs".[1] Therefore, it is particularly important and urgent to develop novel, high-performance antimicrobial agents that can overcome antibiotic resistance. Among the numerous strategies of antibacterial control, the use of reactive oxygen species (ROS) to induce cell oxidative stress response leading to cell death is one of the most advanced, effective bactericidal processes. Metal oxide semiconductors are known as green antibacterial agents because of their ability to produce ROS, in particular, under photoirradiation at appropriate wavelengths.[2,3] For instance, zinc oxide (ZnO) is a unique nontoxic material with high photocatalytic activity and chemical stability.[4−7] However, the wide band gap (3.3 eV) and low photoenergy conversion efficiency of ZnO greatly limit its practical applications.[8] This issue can be mitigated by deliberate structural engineering.[9−12] For instance, it has been observed[13] that cobalt doping into ZnO nanoparticles (CoZnO) can effectively extend the absorption to the visible range and enhance the separation efficiency of photo-generated electron–hole pairs, the structural defects caused by Co doping into ZnO can facilitate the production of ROS, and Zn^{2+} ions released from the ZnO lattice can cause bacterial membrane damage and result in improved bacterial inactivation.

Molybdenum disulfide (MoS_2), a typical p-type layered semiconductor with a narrow band gap (1.9 eV), has also been attracting significant attention, due to its strong absorption in the visible range of the solar spectrum[14] and intrinsic peroxidase-like activity for the detection of H_2O_2 and glucose.[15] In addition, MoS_2 nanosheets exhibit a large surface

Received: October 26, 2020
Accepted: February 25, 2021
Published: March 9, 2021

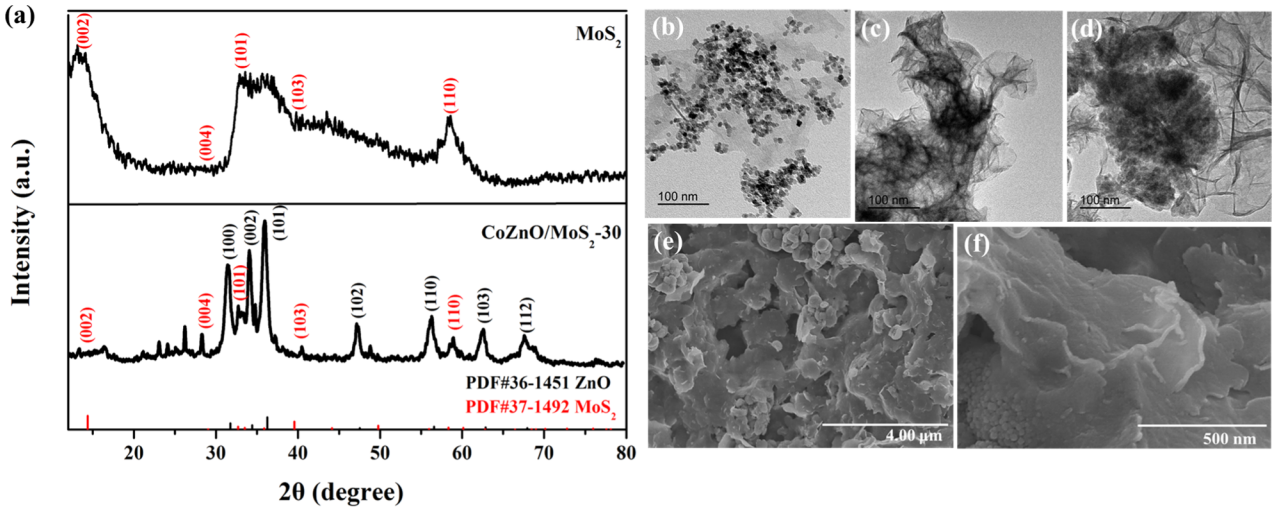

Figure 1. (a) XRD patterns of MoS_2 and CoZnO/MoS_2-30 nanocomposite. TEM images of (b) CoZnO nanoparticles, (c) MoS_2 nanosheets, and (d) CoZnO/MoS_2-30 nanocomposite. (e,f) SEM images of the CoZnO/MoS_2-30 nanocomposite in different magnifications.

area and abundant edges that are conducive to adsorbate surface binding[16,17] and have been used extensively in photocatalysis.[18−20] However, MoS_2 exhibits limited bactericidal activity due to the rapid recombination of photogenerated electron−hole pairs.[21]

In the present study, a deliberate integration of CoZnO nanoparticles and MoS_2 nanosheets is found to lead to the development of functional nanocomposites that can be used as a rapid and broad-spectrum bactericidal agent, due largely to the combined contributions of peroxidase-like activity from MoS_2 and oxidative stress from photo-generated ROS by CoZnO. Remarkably, the CoZnO/MoS_2 nanocomposites show not only evident antibacterial activity toward both Gram-negative and Gram-positive bacteria but also strong inhibition of the growth of fungi. Thus, such functional nanocomposites may find applications in fruit preservation films, antibacterial packages, antibacterial fabrics, and so on.

2. EXPERIMENTAL SECTION

2.1. Chemicals. Zinc acetate dihydrate ($Zn(CH_3COO)_2{\cdot}2H_2O$), sodium carbonate ($Na_2CO_3$), and sodium bicarbonate ($NaHCO_3$) were all obtained from Tianjing Chemical Regents Co., Ltd. Cobalt acetate tetrahydrate ($Co(CH_3COO)_2{\cdot}4H_2O$), L-cysteine, glutathione (GSH), and Tris−HCl buffer ($C_4H_{11}NO_3$) were obtained from Macklin Biochemicals Co., Ltd. Lithium hydroxide (LiOH) and sodium molybdate ($Na_2MoO_4{\cdot}2H_2O$) were purchased from Tianjing Hong Yan Chemical Regents Co., Ltd. 5,5′-Dithiobis-(2-nitrobenzoic acid) (DTNB) was purchased from Hefei BASF Biotechnology Co., Ltd. All chemicals were of analytic reagent grade and used directly without further treatment.

2.2. Preparation of CoZnO/MoS_2 Nanocomposites. MoS_2 nanosheets were prepared by a modified literature procedure.[22] In brief, 0.3 g of sodium molybdate and 0.6 g of L-cysteine were dispersed in 50 mL of deionized water under magnetic stirring for 30 min and then transferred into a Teflon-lined autoclave for hydrothermal treatment at 180 °C for 30 h. The precipitates were collected by centrifugation and rinsed with copious amounts of water, affording purified MoS_2 nanosheets.

To prepare CoZnO/MoS_2 nanocomposites, 1.1 g of zinc acetate ($Zn(CH_3COO)_2{\cdot}2H_2O$) and a calculated amount of cobalt acetate ($Co(CH_3COO)_2{\cdot}4H_2O$, Co/Zn mole ratio = 0.7%) were dispersed in 100 mL of ethanol under magnetic stirring, into which was added a calculated amount of MoS_2 nanosheets prepared above (x = 5, 10, 15, 20, 25, and 30 mg). The mixed solution was heated at 80 °C for 2 h before the addition of 0.3 g of LiOH in ethanol. Finally, deionized water was added dropwise into the solution until a milky white suspension was produced. The precipitates were collected by centrifugation and rinsed with absolute ethanol and deionized water three times, and the purified sample was denoted CoZnO/MoS_2-x. Pure CoZnO nanoparticles were also prepared in the same manner without the addition of MoS_2 nanosheets.

2.3. Characterization. The sample morphologies were examined with a Tecnai G2 F20 S-TWIN transmission electron microscope at the accelerating voltage of 200 kV and an S4800 field-emission scanning electron microscope. X-ray diffraction (XRD) patterns were acquired with a Rigaku D/MAX-2200 diffractometer with Co K_α radiation (λ = 0.179 nm). X-ray photoelectron spectroscopy (XPS) analysis was performed with an AXIS SUPRA spectrometer. Electron spin resonance (ESR) measurements were carried out with a JEOL JES-FA200 instrument at room temperature using 5-dimethyl pyrroline-1-oxide (DMPO) as the spin trap. Zeta potential (ζ) was measured with a Malvern Nano-ZS powder particle size analyzer.

2.4. Minimum Inhibitory Concentration Experiments. The Gram-negative bacterium *Escherichia coli*, Gram-positive bacterium *Staphylococcus Aureus*, and fungus *Aspergillus flavus* were cultured for 24 h in a nutrient agar medium. Three viable colonies were transferred to 1 mL of a phosphate-buffered saline (PBS) solution, and the bacterial turbidity was adjusted to an optical density of 0.01 (OD = 0.01). To determine the nanocomposite minimum inhibitory concentration (MIC) against bacteria or fungi, a series of solutions were prepared in PBS at concentrations ranging from 0.05 to 5.0 mg mL^{-1} with a final volume of 100 μL in each 96-well plate. 5 μL of the test solutions (OD = 0.01) and 5 μL of an agar medium containing the nanocomposites at various concentrations were inoculated into each well, and the optical density was recorded at 37 °C every 10 min for 24 h using the Molecular Devices SpectraMax Plus Microplate reader. The lowest concentration of the nanocomposites that inhibited the growth of the bacteria or fungi was determined as the corresponding MIC.

2.5. Antibacterial Assay. The nanocomposites prepared above were assayed for growth inhibition against various bacterial strains. Briefly, 1 mL of a bacterial suspension (OD = 0.01) was diluted 100 times and added to a plastic centrifuge tube, into which was added 1 mL of the CoZnO/MoS_2 nanocomposite (2.0 mg mL^{-1}) solution in a dropwise fashion. The mixture was then placed in a shaking incubator for 18 h at 37 °C. 25 μL of the resulting suspension was spread onto the nutrient agar medium and incubated at 37 °C for 18 h, while the bacterial inactivation percentage was recorded.

2.6. Photodynamic Antibacterial Performance. 0.5 mL of a bacterial suspension (OD = 0.01, diluted 100 times) was mixed with 0.5 mL of 20 μg mL^{-1} CoZnO/MoS_2 nanocomposites in a 2 mL

https://dx.doi.org/10.1021/acsanm.0c02875
ACS Appl. Nano Mater. 2021, 4, 4361−4370

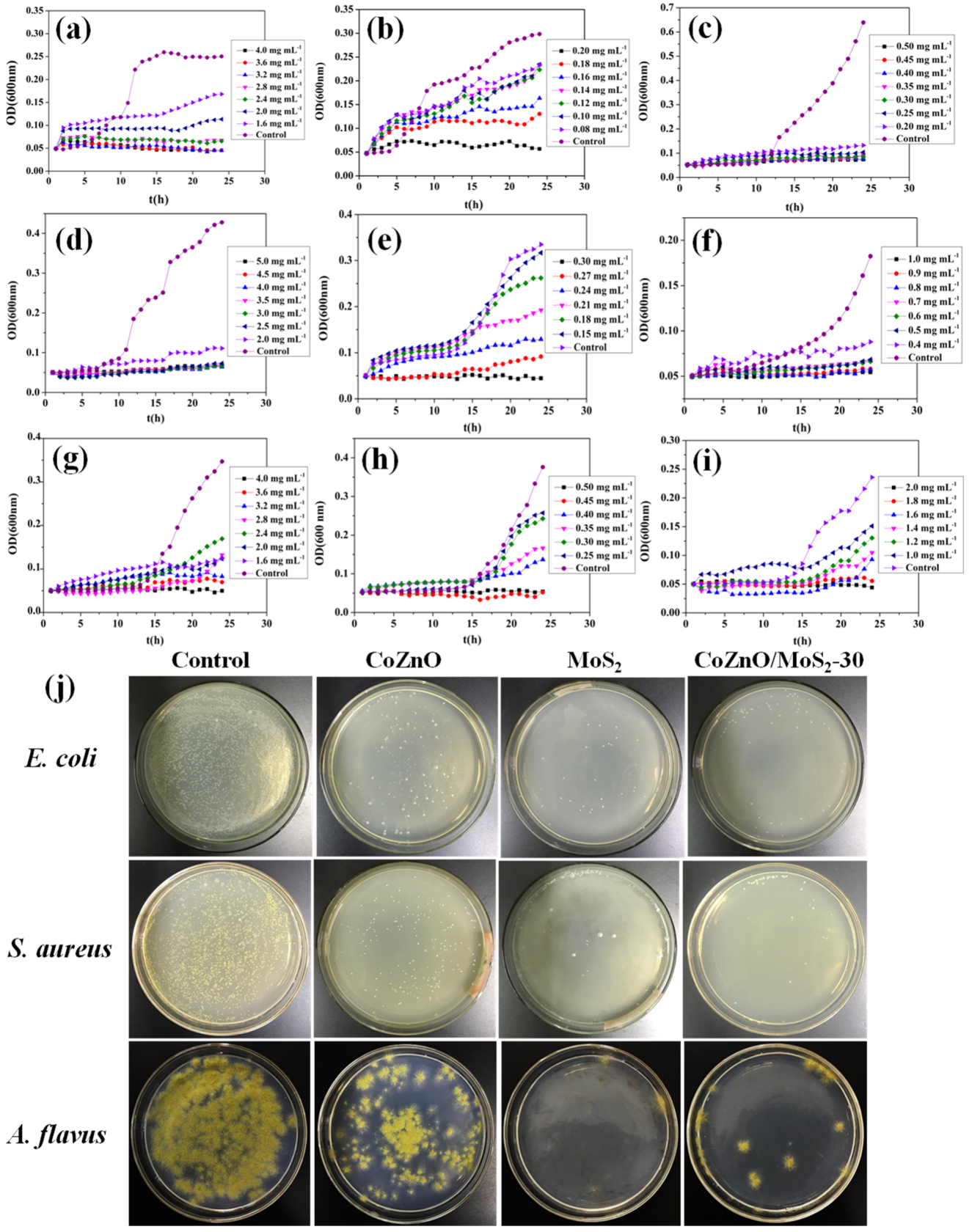

Figure 2. Growth curves in the dark of (a–c) *E. coli*, (d–f) *S. aureus*, and (g–i) *A. flavus* in nutritional broth containing (a,d,g) CoZnO, (b,e,h) MoS_2, and (c,f,i) CoZnO/MoS_2-30 nanocomposites. (j) Photographs of the growth of *E. coli*, *S. aureus*, and *A. flavus* after treatment for 18 h with CoZnO, MoS_2 and CoZnO/MoS_2-30 nanocomposite in the dark.

https://dx.doi.org/10.1021/acsanm.0c02875
ACS Appl. Nano Mater. 2021, 4, 4361–4370

plastic centrifuge tube. After photoirradiation (at 360 nm and 808 nm, 15 W, Shenzhen ChengYu Photoelectric Co., Ltd.) for a selected period of time, 25 μL of the bacterial suspension was evenly coated onto an agar culture medium and incubated at 37 °C for 18 h, allowing for the calculation of cell survival.

2.7. TEM Characterization of Bacterial Cells. 1 mL of the CoZnO/MoS_2 nanocomposites (1.0 mg mL^{-1}) was mixed with 10 mL of *E. coli* (OD = 0.1) in a centrifuge tube, and the mixture was placed in a shaking incubator at 500 rpm for 18 h at 37 °C. The precipitates were collected by centrifugation, re-dispersed in water, and dropcast onto a TEM grid for imaging.[23]

2.8. Intracellular Glutathione Activity. The Ellman method based on GSH oxidation was used to evaluate ROS-independent oxidative stress. 24 225 μL of CoZnO/MoS_2 nanocomposites (160 μg mL^{-1}) and 225 μL of glutathione (1 mM) were dispersed in a bicarbonate buffer (50 mM, pH = 8.7) and oscillated at the speed of 150 rpm for 0.5, 1, 1.5, and 2 h in a shaking incubator at 37 °C, into which 785 μL of Tris−HCl buffer (0.05 M, pH = 8.8) and 15 μL of DTNB (100 mM) were added. The supernatant was collected by centrifugation, and 200 μL of the supernatant was added into the 96-well enzyme marker board, which was placed into the Molecular Devices SpectraMax Plus reader. The wavelength of the enzyme marker was set to 410 nm to assess GSH loss.

3. RESULTS AND DISCUSSION

3.1. Structural Characterization. Figure 1a shows the XRD patterns of MoS_2 and CoZnO/MoS_2-30 nanocomposites.

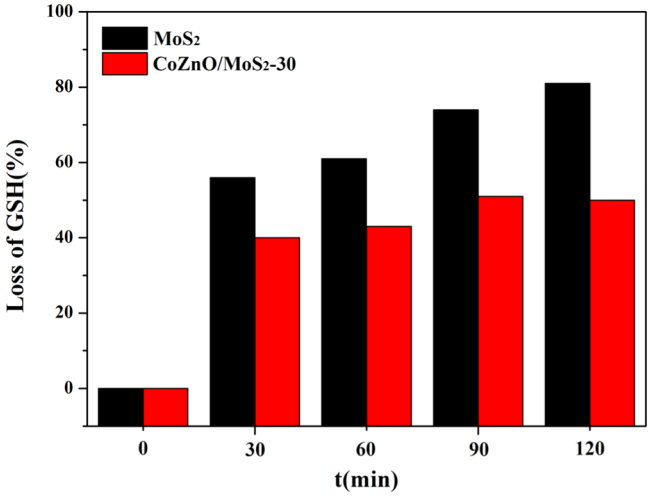

Figure 3. Loss of GSH after treatment with MoS_2 and the CoZnO/MoS_2-30 nanocomposite for different periods of time at 37 °C. The concentrations of CoZnO, MoS_2, and CoZnO/MoS_2-30 are all 0.1 mg mL^{-1}.

One can see that the MoS_2 nanosheets exhibited three major diffraction peaks at 2θ = 14.4, 32.9, and 58.0°, which can be assigned to the (002), (101), and (110) facets of hexagonal phase molybdenum disulfide (JCPDS 37-1492), respectively. The strong (002) diffraction is consistent with a well-defined layered structure.[11] The formation of the CoZnO/MoS_2-30 nanocomposite resulted in additional diffraction peaks at 2θ = 31.71, 34.40, 36.19, 47.45, 56.51, 62.78, and 67.86°, corresponding to the (100), (002), (101), (102), (110), (103) and (112) facets of hexagonal wurtzite ZnO (JCPDS 36-1451). These results indicate successful integration of the two structural components in the composites, which is further confirmed by XPS measurements (Figure S1 and Table S1). Note that no diffraction patterns of metallic cobalt or cobalt oxides can be resolved in the sample.

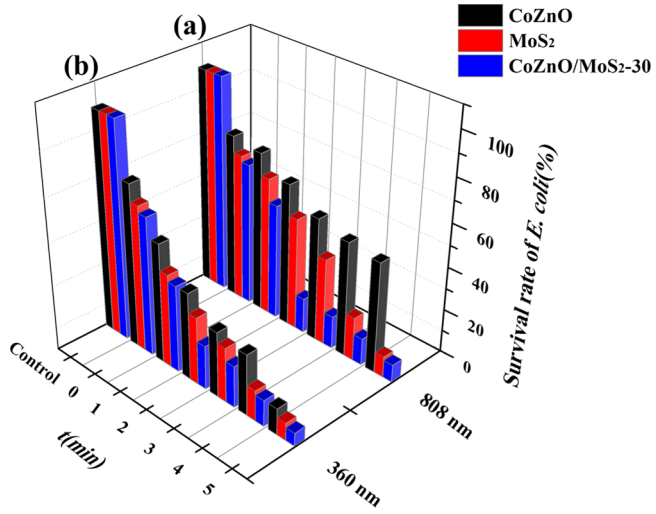

Figure 4. Survival rate of *E. coli* treated with CoZnO, MoS_2, and CoZnO/MoS_2-30 nanocomposite under photoirradiation for up to 5 min at (a) 808 and (b) 360 nm.

The material structures were further characterized by TEM measurements. From Figure 1b, CoZnO nanoparticles can be seen to display a spherical shape with a diameter of about 10 nm, while MoS_2 exhibited a flaky morphology indicating a nanosheet structure, as shown in Figure 1c. In HRTEM measurements (Figure S2a), the MoS_2 nanosheets can be seen to display well-defined lattice fringes with an interplanar distance of about 0.61 nm, consistent with the (002) crystal planes of MoS_2.[25] For the CoZnO/MoS_2-30 nanocomposite (Figure 1d), the CoZnO nanoparticles can be seen to cluster on the MoS_2 surface, with agglomeration intensified at a decreasing CoZnO/MoS_2 feed ratio (Figure S2b−f). This can be accounted for by the high specific surface area and abundant functional groups on the MoS_2 nanosheets that facilitated the interactions with Zn^{2+}.[26−28] Consistent results were obtained in SEM measurements (Figure 1e,f), where the CoZnO/MoS_2-30 nanocomposite is composed of MoS_2 nanosheets and agglomerated CoZnO nanoparticles.[28] In Raman spectroscopic measurements (Figure S3), the CoZnO/MoS_2-30 hybrid can be seen to consist of mixed 1T- and 2H-phases of MoS_2, where the in-plane (E^1_{2g}) and out-of-plane (A_{1g}) vibrations of MoS_2 can be identified at 376 and 402 cm^{-1} (Figure S3 inset), and the separation of 26 cm^{-1} suggests the formation of multiple layers of MoS_2. Taken together, these results confirm the successful preparation of CoZnO/MoS_2 nanocomposites.

3.2. Antibacterial Activity. Figure 2a−c shows the growth curves of *E. coli* cultured for 24 h in the dark in a nutrient broth containing (a) CoZnO, (b) MoS_2, and (c) CoZnO/MoS_2-30 nanocomposites. One can see from Figure 2c that at CoZnO/MoS_2-30 concentrations above 0.20 mg mL^{-1}, the growth of the *E. coli* cells was significantly inhibited, suggesting that the MIC of CoZnO/MoS_2-30 toward *E. coli* was below 0.20 mg mL^{-1}. For other CoZnO/MoS_2 nanocomposites prepared at different MoS_2 feeds (Figure S4), the MICs were estimated to be 0.70 mg mL^{-1} for CoZnO/MoS_2-5, 0.60 mg mL^{-1} for CoZnO/MoS_2-10, 0.45 mg mL^{-1} for CoZnO/MoS_2-15, 0.35 mg mL^{-1} for CoZnO/MoS_2-20, and 0.30 mg mL^{-1} for CoZnO/MoS_2-25, indicative of the increasing inhibition of bacterial growth with increasing MoS_2 feed. For comparison, the MIC was 0.20 mg mL^{-1} for MoS_2 alone (Figure 2b) and markedly higher for CoZnO (2.4 mg mL^{-1}, Figure 2a). These

https://dx.doi.org/10.1021/acsanm.0c02875
ACS Appl. Nano Mater. 2021, 4, 4361−4370

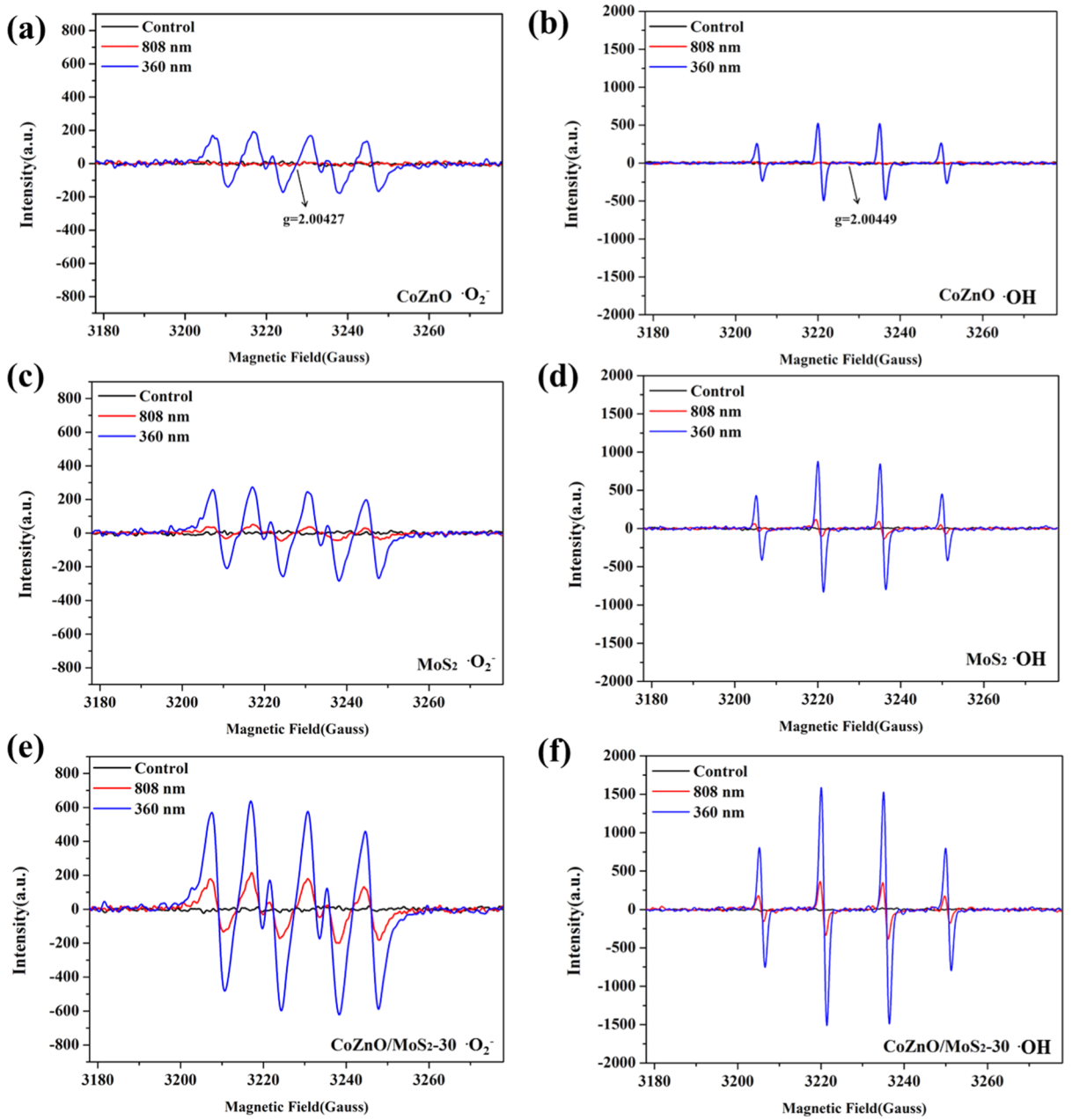

Figure 5. ESR spectra of blank water (control) and dispersions containing different samples under photoirradiation at 808 or 360 nm: (a,b) CoZnO, (c,d) MoS_2, and (e,f) CoZnO/MoS_2-30.

observations suggest that MoS_2 played a dominant role in dictating the antimicrobial activity of the CoZnO/MoS_2 nanocomposites in the dark, likely due to MoS_2's peroxidase-like activity to induce oxidative stress and GSH oxidation that resulted in rapid bacterial death (vide infra).[24]

Similar behaviors were observed toward *Staphylococcus aureus* (Figure 2d–f), where the MIC decreased in the similar order of CoZnO (2.5 mg mL^{-1}) > CoZnO/MoS_2-30 (0.5 mg mL^{-1}) > MoS_2 (0.27 mg mL^{-1}). Notably, the samples also exhibit an apparent inhibitory activity toward the fungus *A. flavus* (Figure 2g–i), with the corresponding MIC of 3.6 mg mL^{-1} for CoZnO, 0.45 mg mL^{-1} for MoS_2 and 1.8 mg mL^{-1} for CoZnO/MoS_2-30 nanocomposites.

Furthermore, the rate constant (k) of bacterial and fungus growth, which was quantified by exponential fitting of the rising part of the growth curves (Figure 2 and S4),[29] diminished drastically upon the addition of CoZnO, MoS_2, and CoZnO/MoS_2 nanocomposites, and was the lowest in the presence of CoZnO/MoS_2-30 nanocomposite (Figure S5).

These results clearly demonstrate the high activity of CoZnO/MoS_2-30 in the inhibition of bacterial and fungus growth, in particular, in comparison to ZnO-based nanocomposites reported recently in the literature.[30,31] Indeed, after 18 h of treatment, one can see that in comparison to the control, the number of bacterial and fungus colonies decreased markedly in the presence of CoZnO, and almost none remained with MoS_2 and CoZnO/MoS_2-30 (Figure 2j).

The different inhibition activity observed above can be correlated to results of GSH oxidation assays. GSH plays an important role in the antioxidant defense system of bacterial cells, which can prevent oxidative stress from damaging cell components. Figure 3 depicts the loss of GSH in the presence

https://dx.doi.org/10.1021/acsanm.0c02875
ACS Appl. Nano Mater. 2021, 4, 4361–4370

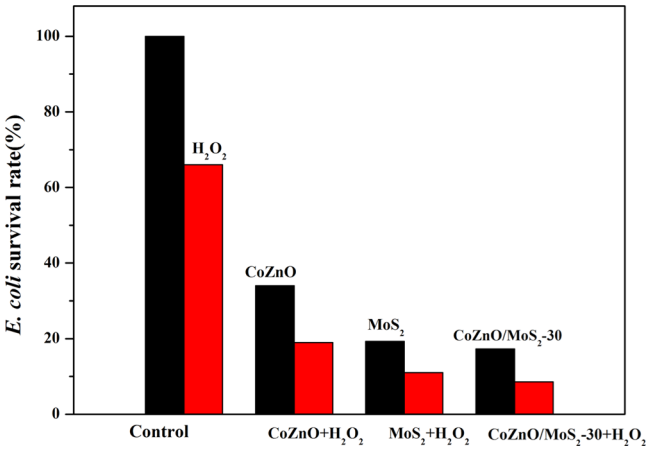

Figure 6. Survival rates of *E. coli* treated by CoZnO, MoS_2, and CoZnO/MoS_2-30 in the absence (black bars) and presence (red bars) of H_2O_2 for 30 min. The concentrations of CoZnO, MoS_2, and CoZnO/MoS_2-30 are all 0.1 mg mL^{-1}.

of MoS_2 and CoZnO/MoS_2-30 nanocomposites. Upon incubation with MoS_2 or CoZnO/MoS_2-30 nanocomposites, the concentration of GSH was found to gradually diminish with increasing incubation time. Interestingly, bare MoS_2 was more effective in inducing GSH oxidation than the CoZnO/MoS_2-30 nanocomposites, likely because GSH oxidation was directly related to the reaction between MoS_2 and the sulfhydryl groups in GSH.[32,33]

The antimicrobial activity was more pronouncedly differentiated under photoirradiation. Based on the above MIC test results, the concentration of the samples was set below the respective MIC in the following photodynamic experiments. Figure 4 shows the survival rate of *E. coli* in the presence of CoZnO (black), MoS_2 (red), and CoZnO/MoS_2-30 nanocomposite (blue). Under red-light photoirradiation (808 nm, Figure 4a), the number of *E. coli* colonies exhibited an apparent decrease in the presence of CoZnO, MoS_2, and CoZnO/MoS_2-30; and the bactericidal activity increased in the order of CoZnO < MoS_2 < CoZnO/MoS_2-30. For instance, after 5 min of photoirradiation, ca. 51% of bacterial cells survived in the presence of CoZnO, while only 9.6% for MoS_2 and 8% for CoZnO/MoS_2-30. A similar trend was observed under photoirradiation of a UV/blue light (360 nm, Figure 4b) but at a much faster rate, suggesting that the CoZnO/MoS_2-30 composites stood out as the most active antimicrobial agent among the series of samples, and more importantly, may serve as a rapid, broad-spectrum bactericidal material.

3.3. Photodynamic Antibacterial Mechanism. To unravel the photodynamic antibacterial mechanism of the CoZnO/MoS_2 nanocomposites, ESR measurements were carried out using DMPO as a spin trap. As can be seen from Figure 5a,b, similar to the control (black curves), no obvious ESR signal was generated with CoZnO under photoirradiation

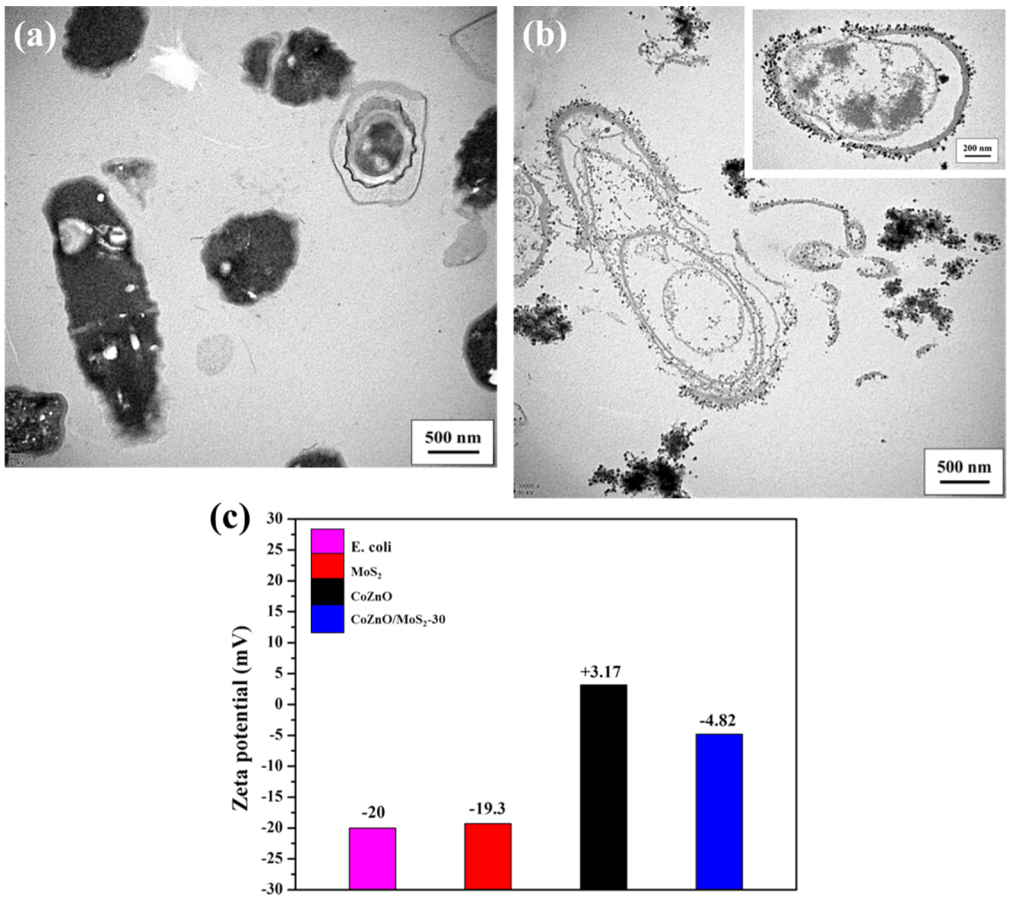

Figure 7. TEM images of (a) untreated *E. coli* cells and (b) *E. coli* cells after the treatment of CoZnO/MoS_2-30 composites. Inset to panel (b) is a TEM image at a high magnification. (c) Zeta potentials of *E. coli* (pink), MoS_2 (red), CoZnO (black) and CoZnO/MoS_2-30 nanocomposite (blue).

https://dx.doi.org/10.1021/acsanm.0c02875
ACS Appl. Nano Mater. 2021, 4, 4361−4370

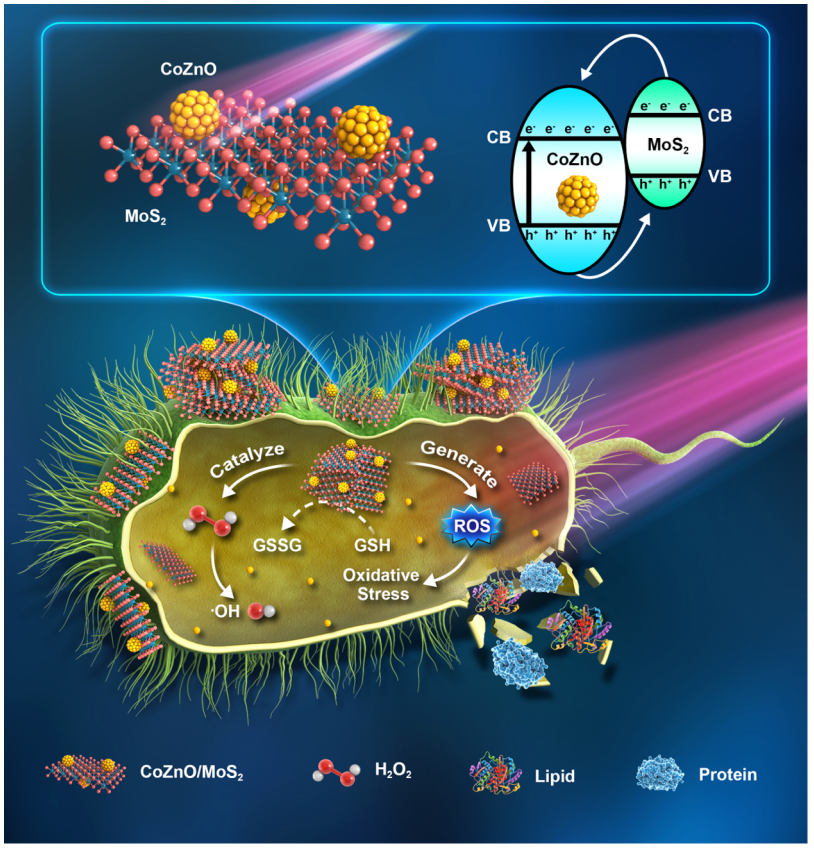

Figure 8. Schematic illustration of the antibacterial process of $CoZnO/MoS_2$ composites.

at 808 nm (red curves), whereas apparent hyperfine features were observed under photoirradiation at 360 nm (blue curves), consistent with the generation of superoxide radicals ($^{\bullet}O_2^-$, g = 2.00427) and hydroxyl radicals ($^{\bullet}OH$, g = 2.00449). Such a discrepancy may be ascribed to the wide band gap of ZnO such that excitation of valence electrons to the conduction band occurs only when the photon energy is sufficiently high.[34]

By sharp contrast, obvious ESR signals, with g = 2.00427 for $^{\bullet}O_2^-$, were produced with MoS_2 and $CoZnO/MoS_2$-30 even under 808 nm photo illumination (Figures 5c–f, red curves), and became markedly intensified under photoirradiation at 360 nm. This can be ascribed to the low band gap of MoS_2,[24] and the fact that the signals were significantly more intense with $CoZnO/MoS_2$-30 than with MoS_2 alone suggests enhanced charge separation in the nanocomposites.[35]

Furthermore, from Figure 5, one can see that $^{\bullet}OH$ was produced at a higher rate than $^{\bullet}O_2^-$. Note that $^{\bullet}OH$ is known to induce oxidative damage of bacterial cell walls and cell membranes, leading to cell death.[12,24] Therefore, the bactericidal activity of CoZnO, MoS_2, and $CoZnO/MoS_2$-30 against *E. coli* was also examined and compared with the addition of low-concentration H_2O_2. From Figure 6, one can see apparent inhibition of the bacterial growth by H_2O_2 alone, and the inhibition was significantly enhanced in the presence of CoZnO, MoS_2, and $CoZnO/MoS_2$-30 nanocomposites. Specifically, the combination of $CoZnO/MoS_2$-30 nanocomposite and H_2O_2 led to a 91.4% inhibition rate of the growth of *E. coli*, a performance better than those of MoS_2 nanosheets (89.0%), CoZnO (81.0%), and H_2O_2 (34%) alone. This suggests that the peroxidase-like activity for H_2O_2 decomposition to hydroxyl radicals increases in the order of CoZnO < MoS_2 < $CoZnO/MoS_2$-30.[24] This was also manifested in the photocatalytic degradation of methyl orange, where $CoZnO/MoS_2$-30 nanocomposites exhibited markedly enhanced activity, as compared to CoZnO and MoS_2, under photoirradiation at 360 or 808 nm (Figures S6 and S7), likely due to the formation of heterojunctions that facilitated the separation of photogenerated electron–hole pairs and the subsequent formation of ROS. Note that H_2O_2 can be produced in vivo by cell metabolism and then decomposed by the $CoZnO/MoS_2$ composites due to their bactericidal activity.[36,37]

Indeed, substantial changes in the *E. coli* cell morphologies can be seen before and after treatment with the $CoZnO/MoS_2$-30 nanocomposite for 18 h. In contrast to untreated *E. coli* that displayed a rod-like shape, smooth cell wall, cell membrane, and cytoplasm (Figure 7a), the addition of $CoZnO/MoS_2$-30 nanocomposite led to apparent damage to the bacterial cells with a clear loss of the structural integrity of the cell walls and cell membranes (Figure 7b), and the shape of the *E. coli* cells became irregular and wrinkled, with apparent leakage of contents within the cytoplasm due to cell wall rupture.[38] This is likely aided by the adsorption of the nanocomposites onto the *E. coli* surface and cellular internalization by the bacteria (inset to Figure 7b), as Mo and S are essential trace elements for various enzymes in the cells.[39]

The adsorption of $CoZnO/MoS_2$-30 nanocomposite onto the bacterial cells is likely driven by the electrostatic interaction between the positively charged CoZnO and negatively charged *E. coli* cells. Figure 7c shows the zeta potentials (ζ) of *E. coli*, MoS_2, CoZnO, and $CoZnO/MoS_2$-30 nanocomposite. One can see that MoS_2 nanosheets exhibited a negative ζ of −19.3

https://dx.doi.org/10.1021/acsanm.0c02875
ACS Appl. Nano Mater. 2021, 4, 4361–4370

mV due to a large number of negatively charged S atoms and functional groups such as −OH and −COOH;[40] and CoZnO was positively charged (ζ = +3.17 mV) because ZnO has a high isoelectric point (pI = 9.5), which makes it easy to combine with low pI materials such as biological macromolecules via electrostatic interactions.[41,42] With the loading of CoZnO onto MoS_2 nanosheets, the resulting CoZnO/MoS_2 nanocomposites exhibited a less negative charge (ζ = −4.82 mV). This suggests that the interactions between the CoZnO/MoS_2 nanocomposites and bacterial cells were most likely facilitated by the CoZnO nanoparticles, which brought the active MoS_2 close to the bacterial cell surface and led to effective bactericidal action (inset to Figure 7b).

Based on the above results, the high antibacterial activity of CoZnO/MoS_2 nanocomposites can be attributed to the combined contributions of high efficiency in ROS production and enhanced electrostatic interactions with the bacterial cell surface. The antibacterial mechanism of the CoZnO/MoS_2 nanocomposite is schematically illustrated in Figure 8. First, the intimate interactions between MoS_2 nanosheets and CoZnO nanoparticles significantly improved the separation efficiency of photo-generated electron−hole pairs and the subsequent production of ROS.[43] Second, the strong electrostatic attraction between CoZnO and bacterial cells boosted the adsorption of the composite onto the cell surface.[44] In addition, the accumulation of CoZnO/MoS_2 nanocomposites on the cell surface hindered the physical mobility of the cell membrane, resulting in membrane damage and cytoplasmic leakage.[45] Furthermore, the photochemical reaction of the CoZnO/MoS_2 nanocomposites resulted in the production of a large number of ROS, where hydroxyl radicals might be produced both in the interior of the bacterial cell and outside of the cell. This leads to a significant GSH loss, which compromised the antioxidant defense system and led to bacterial cell death.[46]

4. CONCLUSIONS

In this study, CoZnO/MoS_2 nanocomposites were prepared by a facile wet-chemistry method and exhibited markedly enhanced antimicrobial activity toward Gram-negative and Gram-positive bacteria and a fungus, as compared to CoZnO nanoparticles and MoS_2 nanosheets alone, under photoirradiation at 360 and 808 nm. This was accounted for by the combined contributions of (i) the peroxidase-like activity of MoS_2 that facilitated the production of hydroxyl radicals and (ii) the enhanced separation efficiency of photogenerated electron−hole pairs that most likely originated from the formation of CoZnO/MoS_2 heterojunctions, leading to enhanced formation of ROS. The produced ROS remarkably accelerated the breakdown of bacterial cell membranes and intracellular glutathione oxidation, destroying the antioxidant defense system of bacteria, thus resulting in broad-spectrum antimicrobial efficiency. Such bactericidal actions were likely aided by the electrostatic interaction between CoZnO/MoS_2 nanocomposites and the bacterial cell surface that enriched the nanocomposites in the proximity of the cells. The results of this work offer new fundamental insights into the rational design and engineering of CoZnO/MoS_2-based nanocomposites as low-cost, high-efficiency, and broad-spectrum antibacterial agents.

■ ASSOCIATED CONTENT

Supporting Information

The Supporting Information is available free of charge at https://pubs.acs.org/doi/10.1021/acsanm.0c02875.

Summary of sample elemental compositions based on the results of XPS studies, XPS full spectrum and high-resolution scans of all the elements of the CoZnO/MoS_2-30 nanocomposite, HRTEM images of MoS_2 nanosheets and CoZnO/MoS_2 nanocomposites, Raman spectra of MoS_2 and the CoZnO/MoS_2-30 nanocomposite, growth curves of E. coli in the dark in a nutritional broth containing CoZnO/MoS_2 nanocomposites at varied concentrations, kinetic analysis of bacterial and fungus cell inactivation with different samples, UV−vis absorption spectra of MoS_2 and the CoZnO/MoS_2-30 nanocomposite, and photocatalytic degradation of methyl orange, CoZnO, and CoZnO/MoS_2 nanocomposites under various conditions (PDF)

■ AUTHOR INFORMATION

Corresponding Authors

Junli Liu − *School of Materials Science and Engineering, Shaanxi Key Laboratory of Green Preparation and Functionalization for Inorganic Materials, Shaanxi University of Science & Technology, Xi'an, Shaanxi 710021, China;* orcid.org/0000-0003-0699-4619; Email: liujunli042@163.com

Shaowei Chen − *Department of Chemistry and Biochemistry, University of California, Santa Cruz, California 96064, United States;* orcid.org/0000-0002-3668-8551; Email: shaowei@ucsc.edu

Authors

Wenxia Cheng − *School of Materials Science and Engineering, Shaanxi Key Laboratory of Green Preparation and Functionalization for Inorganic Materials, Shaanxi University of Science & Technology, Xi'an, Shaanxi 710021, China*

Yuhan Wang − *School of Materials Science and Engineering, Shaanxi Key Laboratory of Green Preparation and Functionalization for Inorganic Materials, Shaanxi University of Science & Technology, Xi'an, Shaanxi 710021, China*

Xiuyi Fan − *School of Materials Science and Engineering, Shaanxi Key Laboratory of Green Preparation and Functionalization for Inorganic Materials, Shaanxi University of Science & Technology, Xi'an, Shaanxi 710021, China*

Jiahao Shen − *School of Materials Science and Engineering, Shaanxi Key Laboratory of Green Preparation and Functionalization for Inorganic Materials, Shaanxi University of Science & Technology, Xi'an, Shaanxi 710021, China*

Hui Liu − *School of Materials Science and Engineering, Shaanxi Key Laboratory of Green Preparation and Functionalization for Inorganic Materials, Shaanxi University of Science & Technology, Xi'an, Shaanxi 710021, China;* orcid.org/0000-0002-5966-1191

Aiqin Wang − *Key Laboratory of Clay Mineral Applied Research of Gansu Province, Center of Eco-Materials and Green Chemistry, Lanzhou Institute of Chemical Physics and Center of Xuyi Palygorskite Applied Technology, Lanzhou*

https://dx.doi.org/10.1021/acsanm.0c02875
ACS Appl. Nano Mater. 2021, 4, 4361−4370

Institute of Chemical Physics, Chinese Academy of Sciences, Lanzhou, Gansu 730000, China; orcid.org/0000-0002-9963-7460

Aiping Hui − *Key Laboratory of Clay Mineral Applied Research of Gansu Province, Center of Eco-Materials and Green Chemistry, Lanzhou Institute of Chemical Physics and Center of Xuyi Palygorskite Applied Technology, Lanzhou Institute of Chemical Physics, Chinese Academy of Sciences, Lanzhou, Gansu 730000, China*

Forrest Nichols − *Department of Chemistry and Biochemistry, University of California, Santa Cruz, California 96064, United States*

Complete contact information is available at: https://pubs.acs.org/10.1021/acsanm.0c02875

Notes

The authors declare no competing financial interest.

■ ACKNOWLEDGMENTS

This work was supported by National Natural Science Foundation of China for Young Scholars (51802185), R&D Center of Xuyi Palygorskite Applied Technology Lanzhou Institute of Chemical Physics, Chinese Academy of Sciences (LICPXY2019-01), and Shaanxi Province Innovation Ability Support Plan-Youth Science and Technology New Stars (S2020-ZC-XXXM-0081). S.W.C. thanks the National Science Foundation (CBET-1848841) for partial support of the work.

■ REFERENCES

(1) Knight, J. Superbugs Reveal Chink in Armour. *Nature* **2002**, *417*, 477.

(2) Yang, B.; Chen, Y.; Shi, J. Reactive Oxygen Species (ROS)-Based Nanomedicine. *Chem. Rev.* **2019**, *119*, 4881−4985.

(3) Ravichandran, K.; Nithiyadevi, K.; Sakthivel, B.; Arun, T.; Sindhuja, E.; Muruganandam, G. Synthesis of ZnO:Co/rGO Nanocomposites for Enhanced Photocatalytic and Antibacterial Activities. *Ceram. Int.* **2016**, *42*, 17539−17550.

(4) Jule, L. T.; Dejene, F. B.; Ali, A. G.; Roro, K. T.; Hegazy, A.; Allam, N. K.; El Shenawy, E. Wide Visible Emission and Narrowing Band Gap in Cd-Doped ZnO Nanopowders Synthesized via Sol-Gel Route. *J. Alloys Compd.* **2016**, *687*, 920−926.

(5) Zhang, X.; Dong, S.; Zhou, X.; Yan, L.; Chen, G.; Dong, S.; Zhou, D. A facile one-pot synthesis of Er-Al co-doped ZnO nanoparticles with enhanced photocatalytic performance under visible light. *Mater. Lett.* **2015**, *143*, 312−314.

(6) Liu, J.; Wang, Y.; Ma, J.; Peng, Y.; Wang, A. A Review on Bidirectional Analogies between the Photocatalysis and Antibacterial Properties of ZnO. *J. Alloys Compd.* **2019**, *783*, 898−918.

(7) Applerot, G.; Lipovsky, A.; Dror, R.; Perkas, N.; Nitzan, Y.; Lubart, R.; Gedanken, A. Enhanced Antibacterial Activity of Nanocrystalline ZnO Due to Increased ROS-Mediated Cell Injury. *Adv. Funct. Mater.* **2009**, *19*, 842−852.

(8) Baviskar, P. K.; Zhang, J. B.; Gupta, V.; Chand, S.; Sankapal, B. R. Nanobeads of Zinc Oxide with Rhodamine B Dye as a Sensitizer for Dye Sensitized Solar Cell Application. *J. Alloys Compd.* **2012**, *510*, 33−37.

(9) TürkyLmaz, E. E.; Güy, N.; Özacar, M. Photocatalytic efficiencies of Ni, Mn, Fe and Ag Doped ZnO Nanostructures Synthesized by Hydrothermal Method: The Synergistic/Antagonistic Effect between ZnO and Metals. *J. Photochem. Photobiol., A* **2017**, *341*, 39−50.

(10) Anitha, S.; Muthukumaran, S. Structural, Optical and Antibacterial Investigation of La, Cu Dual Doped ZnO Nanoparticles Prepared by co-Precipitation Method. *Mater. Sci. Eng., C* **2019**, *108*, 110387.

(11) Tan, Y. H.; Yu, K.; Li, J. Z.; Fu, H.; Zhu, Z. Q. MoS_2@ZnO Nano-Heterojunctions with Enhanced Photocatalysis and Field Emission Properties. *J. Appl. Phys.* **2014**, *116*, 643051−643059.

(12) Liu, J.; Rojas-Andrade, M. D.; Chata, G.; Peng, Y.; Roseman, G.; Lu, J.-E.; Millhauser, G. L.; Saltikov, C.; Chen, S. Photo-Enhanced Antibacterial Activity of ZnO/Graphene Quantum Dot Nanocomposites. *Nanoscale* **2018**, *10*, 158−166.

(13) Liu, J.; Wang, Y.; Shen, J.; Liu, H.; Li, J.; Wang, A.; Hui, A.; Munir, H. A. Superoxide Anion: Critical Source of High Performance Antibacterial Activity in Co-Doped ZnO QDs. *Ceram. Int.* **2020**, *46*, 15822−15830.

(14) Chen, S. F.; Wu, Y. R. A Design of Intermediate Band Solar Cell for Photon Ratchet with Multi-layer MoS_2 Nanoribbons. *Appl. Phys. Lett.* **2017**, *110*, 5014−5943.

(15) Roy, S.; Mondal, A.; Yadav, V.; Sarkar, A.; Banerjee, R.; Sanpui, P.; Jaiswal, A. Mechanistic Insight into the Antibacterial Activity of Chitosan Exfoliated MoS_2 Nanosheets: Membrane Damage, Metabolic Inactivation, and Oxidative Stress. *ACS Appl. Bio Mater.* **2019**, *2*, 2738−2755.

(16) Theerthagiri, J.; Senthil, R. A.; Senthilkumar, B.; Reddy Polu, A.; Madhavan, J.; Ashokkumar, M. Recent advances in MoS_2 nanostructured materials for energy and environmental applications - A review. *J. Solid State Chem.* **2017**, *252*, 43−71.

(17) Liu, Y.; Pan, J.; Li, H.; Ou, W.; Li, S.; Zhao, W.; Wang, J.; Song, C.; Zheng, Y.; Li, C. The 2D petaloid MoS_2 lamellas modified cubic $CaTiO_3$ nanocomposites towards photocatalytic hydrogen production enhancement. *J. Alloys Compd.* **2019**, *811*, 152067.

(18) Tian, X.; Sun, Y.; Fan, S.; Boudreau, M. D.; Chen, C.; Ge, C.; Yin, J. J. Photogenerated Charge Carriers in Molybdenum Disulfide Quantum Dots with Enhanced Antibacterial Activity. *ACS Appl. Mater. Interfaces* **2019**, *11*, 4855−4866.

(19) Xu, J.; Gulzar, A.; Liu, Y.; Bi, H.; Gai, S.; Liu, B.; Yang, D.; He, F.; Yang, P. Integration of IR-808 Sensitized Upconversion Nanostructure and MoS_2 Nanosheet for 808 nm NIR Light Triggered Phototherapy and Bioimaging. *Small* **2017**, *13*, 1701841.

(20) Liu, C.; Kong, D.; Hsu, P.-C.; Yuan, H.; Lee, H.-W.; Liu, Y.; Wang, H.; Wang, S.; Yan, K.; Lin, D.; Maraccini, P. A.; Parker, K. M.; Boehm, A. B.; Cui, Y. Rapid water disinfection using vertically aligned MoS_2 nanofilms and visible light. *Nat. Nanotechnol.* **2016**, *11*, 1098−1104.

(21) Shanmugam, V.; Jeyaperumal, K. S.; Mariappan, P.; Muppudathi, A. L. Fabrication of novel g-C_3N_4 based MoS_2 and Bi_2O_3 nanorod embedded ternary nanocomposites for superior photocatalytic performance and destruction of bacteria. *New J. Chem.* **2020**, *44*, 13182−13194.

(22) Li, X.; He, D. W.; Wang, Y. S.; Hu, Y.; Zhao, X.; Fu, C.; Wu, J. Y. Facile and Controllable Synthesis of Molybdenum Disulfide Quantum Dots for Highly Sensitive and Selective Sensing of Copper Ions. *Chin. Phys. B* **2018**, *5*, 423−427.

(23) Liu, J.; Shao, J.; Wang, Y.; Li, J.; Liu, H.; Wang, A.; Hui, A.; Chen, S. Antimicrobial Activity of Zinc Oxide-Graphene Quantum Dot Nanocomposites: Enhanced Adsorption on Bacterial Cells by Cationic Capping Polymers. *ACS Sustain. Chem. Eng.* **2019**, *7*, 16264−16273.

(24) Yin, W.; Yu, J.; Lv, F.; Yan, L.; Zheng, L. R.; Gu, Z.; Zhao, Y. Functionalized Nano-MoS_2 with Peroxidase Catalytic and Near-Infrared Photothermal Activities for Safe and Synergetic Wound Antibacterial Applications. *ACS Nano* **2016**, *10*, 11000−11011.

(25) Li, X.-L.; Li, Y.-D. MoS_2Nanostructures: Synthesis and Electrochemical Mg^{2+} Intercalation. *J. Phys. Chem. B* **2004**, *108*, 13893−13900.

(26) Frieden, E. New Perspectives on the Essential Trace Elements. *J. Chem. Educ.* **1985**, *62*, 917−923.

(27) Awasthi, G. P.; Adhikari, S. P.; Ko, S.; Kim, H. J.; Park, C. H.; Kim, C. S. Facile synthesis of ZnO flowers modified graphene like MoS_2 sheets for enhanced visible-light-driven photocatalytic activity and antibacterial properties. *J. Alloys Compd.* **2016**, *682*, 208−215.

(28) Chacko, L.; Poyyakkara, A.; Kumar, V. B. S.; Aneesh, P. M. MoS_2-ZnO nanocomposites as highly functional agents for anti-

angiogenic and anti-cancer theranostics. *J. Mater. Chem. B* **2018**, *6*, 3048−3057.
(29) Rojas-Andrade, M.; Cho, A. T.; Hu, P.; Lee, S. J.; Deming, C. P.; Sweeney, S. W.; Saltikov, C.; Chen, S. Enhanced Antimicrobial Activity with Faceted Silver Nanostructures. *J. Mater. Sci.* **2015**, *50*, 2849−2858.
(30) Danial, E. N.; Hjiri, M.; Abdel-wahab, M. S.; Alonizan, N. H.; El Mir, L.; Aida, M. S. Antibacterial Activity of In-Doped ZnO Nanoparticles. *Inorg. Chem. Commun.* **2020**, *122*, 108281.
(31) Karthik, R.; Thambidurai, S. Synthesis of Cobalt Doped ZnO/Reduced Graphene Oxide Nanorods as Active Material for Heavy Metal Ions Sensor and Antibacterial Activity. *J. Alloys Compd.* **2017**, *715*, 254−265.
(32) Chen, X.; Berner, N. C.; Backes, C.; Duesberg, G. S.; Mcdonald, A. R. Functionalization of Two-Dimensional MoS_2: On the Reaction Between MoS_2 and Organic Thiols. *Angew. Chem., Int. Ed. Engl.* **2016**, *55*, 5803−5808.
(33) Chen, X.; McGlynn, C.; McDonald, A. R. Two-Dimensional MoS_2 Catalyzed Oxidation of Organic Thiols. *Chem. Mater.* **2018**, *30*, 6978−6982.
(34) Sirelkhatim, A.; Mahmud, S.; Seeni, A.; Kaus, N. H. M.; Ann, L. C.; Bakhori, S. K. M.; Hasan, H.; Mohamad, D. Review on Zinc Oxide Nanoparticles: Antibacterial Activity and Toxicity Mechanism. *Nano-Micro Lett.* **2015**, *7*, 219−242.
(35) Li, H.; Shen, H.; Duan, L.; Liu, R.; Li, Q.; Zhang, Q.; Zhao, X. Enhanced photocatalytic activity and synthesis of ZnO nanorods/MoS_2 composites. *Superlattices Microstruct.* **2018**, *117*, 336−341.
(36) Cao, F.; Zhang, L.; Wang, H.; You, Y.; Wang, Y.; Gao, N.; Ren, J.; Qu, X. Defect-Rich Adhesive Nanozymes as Efficient Antibiotics for Enhanced Bacterial Inhibition. *Angew. Chem., Int. Ed.* **2019**, *58*, 16236−16242.
(37) Yu, J.; Ma, X.; Yin, W.; Gu, Z. Synthesis of PVP-functionalized ultra-small MoS_2 nanoparticles with intrinsic peroxidase-like activity for H_2O_2 and glucose detection. *RSC Adv.* **2016**, *6*, 81174−81183.
(38) Zhao, R.; Kong, W.; Sun, M.; Yang, Y.; Liu, W.; Lv, M.; Song, S.; Wang, L.; Song, H.; Hao, R. Highly Stable Graphene-Based Nanocomposite (GO-PEI-Ag) with Broad-Spectrum, Long-Term Antimicrobial Activity and Antibiofilm Effects. *ACS Appl. Mater. Interfaces* **2018**, *10*, 17617−17629.
(39) Cao, F.; Ju, E.; Zhang, Y.; Wang, Z.; Liu, C.; Li, W.; Huang, Y.; Dong, K.; Ren, J.; Qu, X. An Efficient and Benign Antimicrobial Depot Based on Silver-Infused MoS_2. *ACS Nano* **2017**, *11*, 4651−4659.
(40) Dong, Y.; Shao, J.; Chen, C.; Li, H.; Wang, R.; Chi, Y.; Lin, X.; Chen, G. Blue Luminescent Graphene Quantum Dots and Graphene Oxide Prepared by Tuning the Carbonization Degree of Citric Acid. *Carbon* **2012**, *50*, 4738−4743.
(41) Beitollahi, H.; Tajik, S.; Garkani Nejad, F.; Safaei, M. Recent Advances in ZnO Nanostructure-Based Electrochemical Sensors and Biosensors. *J. Mater. Chem. B* **2020**, *8*, 5826−5844.
(42) Soyoon, S.; Ramadoss, A.; Saravanakumar, B.; Kim, S. J. Novel Cu/CuO/ZnO Hybrid Hierarchical Nanostructures for Non-enzymatic Glucose Sensor Application. *J. Electroanal. Chem.* **2014**, *717*−*718*, 90−95.
(43) Wei, M.; Chen, C. S.; Liu, X. Y.; Yang, Z.; Ding, F.; Chao, Z. S.; Liu, T. J. Low-temperature Construction of MoS_2 Quantum Dots/ZnO Spheres and their Photocatalytic Activity under Natural Sunlight. *J. Colloid Interface Sci.* **2018**, *530*, 714−724.
(44) Cho, E. C.; Xie, J.; Wurm, P. A.; Xia, Y. Understanding the Role of Surface Charges in Cellular Adsorption versus Internalization by Selectively Removing Gold Nanoparticles on the Cell Surface with a I2/KI Etchant. *Nano Lett.* **2009**, *9*, 1080.
(45) Zhao, R.; Lv, M.; Li, Y.; Sun, M.; Kong, W.; Wang, L.; Song, S.; Fan, C.; Jia, L.; Qiu, S.; Sun, Y.; Song, H.; Hao, R. Stable Nanocomposite Based on PEGylated and Silver Nanoparticles Loaded Graphene Oxide for Long-Term Antibacterial Activity. *ACS Appl. Mater. Interfaces* **2017**, *9*, 15328−15341.
(46) Ma, J.; Liu, J.; Bao, Y.; Zhu, Z.; Wang, X.; Zhang, J. Synthesis of Large-scale Uniform Mulberry-like ZnO Particles with Microwave Hydrothermal Method and Its Antibacterial Property. *Ceram. Int.* **2013**, *39*, 2803−2810.

https://dx.doi.org/10.1021/acsanm.0c02875
ACS Appl. Nano Mater. 2021, 4, 4361−4370